Materialia 21 (2022) 101337

Contents lists available at ScienceDirect

Materialia

journal homepage: www.elsevier.com/locate/mtla

Selective electrochemical deposition of indium in-between silicon nanowire arrays fabricated by metal-assisted chemical etching

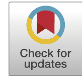

Nikita Grevtsov [a,*], Eugene Chubenko [a], Vladimir Petrovich [a], Vitaly Bondarenko [a], Ilya Gavrilin [b], Alexey Dronov [b], Sergey Gavrilov [b]

[a] Belarusian State University of Informatics and Radioelectronics, Minsk, Belarus
[b] National Research University of Electronic Technology, Zelenograd, Moscow, Russia

ARTICLE INFO

Keywords:
Electrodeposition
Fusible metals
Porous silicon
Silicon nanowires
Metal-assisted chemical etching

ABSTRACT

Indium electrodeposition in-between silicon nanowire arrays fabricated by silver-assisted chemical etching of lightly-doped (100)-oriented silicon wafers is evaluated. It is concluded based on SEM and EDX analysis of indium's distribution that, by utilizing pulsed-mode electrodeposition and maintaining a sufficiently low duty cycle value, indium particles can be formed exclusively at the very bottom of each consecutive pore on the residual silver particles left over from metal-assisted etching. This result differs significantly from irregular pore filling along with surface and subsurface deposition observed in the cases of continuous galvanostatic deposition regimes at prolonged durations or in the absence of residual silver particles. Bottommost fusible metal deposit localization, which is unattainable on porous silicon fabricated by electrochemical anodization, is presumed to be optimal for the growth of germanium crystallites inside the pores via the electrochemical liquid-liquid-solid approach and subsequent silicon-germanium alloy formation through thermal annealing.

1. Introduction

The open cavities and very large surface area of porous silicon (PS) offer tempting prospects for its use as a structural matrix to create various nanocomposites and alloys [1]. PS layers can be formed on silicon substrates by a variety of electrochemical and chemical processing techniques, the most common one being electrochemical anodization in HF solutions [2]. To obtain PS-based nanocomposites and compounds, various metals and their alloys can be deposited into the pore channels [1]. From a practical point of view, deposition of semiconductors into PS also presents a significant interest. Presumably, PS filled with germanium can be used to fabricate Si_xGe_{1-x} alloys by means of its thermal processing. However, a necessary and yet lacking prerequisite to such an approach would be a reproducible way of filling the pore channels with germanium crystallites, which is not possible via conventional electrodeposition. Film structures based on Si_xGe_{1-x} alloys are widely utilized in thermoelectric converters with high stability and thermoelectric efficiency in the temperature range of 800–1100 °C, which allows them to be used in a wide area of applications, ranging from heat utilization during various high-temperature processes to the use in the space exploration equipment [3, 4]. Due to the high cost of crystalline Ge and its gaseous precursors, compositions with low Ge concentration are commonly used to produce Si_xGe_{1-x} (e.g., $Si_{0.8}Ge_{0.2}$), which do not exhibit optimal electrophysical and physicochemical parameters for effective thermoelectric conversion. Thus, at this time the development of a new relatively inexpensive approach to obtaining Si_xGe_{1-x} layers that allows wide-range control over the components' quantity ratios without significantly affecting the cost remains a crucial task.

One of the most interesting recent developments relating to the acquisition of crystalline germanium is the so-called electrochemical liquid-liquid-solid growth (ec-LLS). This process enables deposition of semiconductor (germanium [5–8], silicon [9, 10] or GaAs [11]) crystallites using preliminarily formed fusible metal particles. Indium is considered to be one of the most suitable materials for the fusible metal role [5, 6]. During ec-LLS the fusible metal particles simultaneously act as (a) microscopic cathodes (electron sources) whereat the oxidized semiconductor precursor (e.g., GeO_2) is electrochemically reduced to a zero-valent state, (b) nucleation points where the semiconductor crystals nucleate and (c) reagents (for multicomponent semiconductors such as GaAs). As a result, semiconductor crystal growth occurs underneath each metal particle, usually pushing the latter upwards as the process goes on and forming a semiconductor wire directly below it [5].

* Corresponding author.
E-mail address: hrautsou@gmail.com (N. Grevtsov).

https://doi.org/10.1016/j.mtla.2022.101337
Received 8 November 2021; Accepted 16 January 2022
Available online 19 January 2022
2589-1529/© 2022 Acta Materialia Inc. Published by Elsevier B.V. All rights reserved.

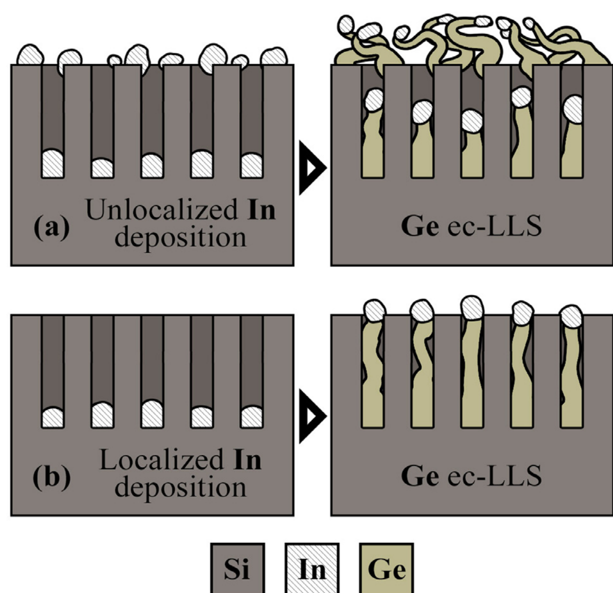

Fig. 1. Hypothetical germanium ec-LLS growth results in two primary cases of preliminarily deposited indium particle layouts: (a) indium particles are present both at the pore bottoms and on the surface; (b) indium particles are strictly localized at the pore bottoms.

While plentiful results have been published regarding the realization of ec-LLS on flat conductive substrates, porous materials are significantly less explored in this regard, and relevant data is nearly non-existent. In a perfect case scenario, metallic indium would have to be deposited selectively into the pores of the PS matrix, and preferably completely localized at the bottom of each consecutive pore [12–14]. Since the crystal growth would be confined by the pore sidewalls, a carefully timed process would result in uniform pore filling with germanium, as illustrated by Fig. 1. If such a structure is exposed to high temperatures by means of thermal annealing, formation of a Si_xGe_{1-x} alloy layer is to be expected, with the quantity ratio of its components being directly dependent on both the annealing parameters and the structural characteristics of the initial porous matrix.

Achieving this manner of fusible metal deposit localization does not pose a simple task, as electrodeposition of metals (such as nickel [12–17], cobalt [13, 18], iron [14], copper [19] and various noble metals [1, 20–22]) into anodic PS (i.e., PS formed by electrochemical anodization in HF solutions), with minor exceptions [23], has been shown to generally result in the nucleation and growth of metal clusters and films either over the entirety of the porous layer or exclusively in its topmost parts. Pulsed electrodeposition is widely used to improve the pore filling factor in cases such as this [24], but complete localization of metal clusters strictly at the pore bottoms was not achieved as of yet due to the need of taking into account the complex combination of silicon and electrolyte conductivity, diffusion limitations and capillary effects, wettability and deposition regime parameters [18]. PS with larger pore diameters, while notably easier to fill [19], is less suitable for effective acquisition of Si_xGe_{1-x} alloys via ec-LLS, as the large sizes of PS's skeleton crystallites could prevent the mixing of Si and Ge at microlevel during their thermal treatment, and formation of elementary Si/Ge semiconductor microclusters can be expected.

In our previous works [25, 26] we have demonstrated that indium can be electrodeposited into anodic PS layers. However, indium crystallites (particles) are formed not only at the pore bottoms, but also at the pore sidewalls and the surface of PS as well [25]. The various approaches we have undertaken to localize the deposition at pore bottoms have not yet been successful [26]. As mentioned before, it was also noted that the kinetics of indium's electrodeposition differ significantly from those of other typically electrodeposited metals, showcasing lacking wettability of the silicon's surface that prevents formation of continuous films and reproducible pore filling [18, 27].

Arrays of vertically-aligned silicon nanowires (SiNWs) present a noteworthy alternative to anodic PS while, under certain processing conditions, maintaining very similar structural parameters well-suitable for subsequent Si-Ge alloy formation [28]. Their main advantage, however, ties close together with the method chosen for their preparation – a technique usually referred to as metal-assisted chemical etching (MACE) that utilizes the catalytic nature of noble metal particles to rapidly accelerate chemical HF-induced etching of silicon directly underneath and/or around them [29]. In other words, noble metal particles deposited onto a silicon wafer preliminarily (two-stage MACE) or simultaneously (one-stage MACE) with its chemical etching in HF act as a mask for the latter, directly dictating the shape and size of the forming cavities and enabling the fabrication of porous structures with a desired morphology [30]. While the residual noble metal particles at the bottoms of the newly-formed pores, if not preliminarily removed, would normally provide difficulties for further applying the resulting structures, they are most advantageous in our specific case, as the ensuing electrodeposition of indium would likely result in its nucleation on the metal particles' surfaces instead of the significantly less conductive silicon wires above them, especially if the latter are prepared on lightly-doped silicon wafers. This hypothesis is further reinforced by the band-bending that would occur at the Schottky junction at the silicon-silver interface: in the case of p-type silicon the band-bending would cause the holes to be pulled away from the wafer's surface [31], slowing down the wafer's oxidation and additionally promoting the reduction of indium ions.

Taking the above into consideration, the structures in question can be deemed promising as substrates that provide favorable conditions for subsequent ec-LLS growth of Ge and fabrication of Si_xGe_{1-x} alloys. While a similar approach has been previously assessed by C. Lee et al. [32] in regards to filling pores created by gold-assisted chemical etching with copper, only the filling of single vertically-aligned pores has been observed as opposed to reproducible filling of arrays thereof, and large-scale copper deposits were also present on the surface of the porous layer, which is extremely undesirable for our specific use case. It has also been shown by S. Yae et al. [33] that employing MACE prior to depositing metal films greatly improves the latter's surface adhesion, but neither the nature nor the reproducibility of pore filling have been evaluated. Conformal deposition of metals onto MACE-produced nanowires was reported by T. Ozel [et al.], resulting in the formation of core-shell structures [34]. A more complex approach to what could be described as localized pore filling has also been evaluated F. Wendisch [et al.] who employed three-dimensional electrochemical axial lithography in conjunction with MACE in order to form SiNWs with SiO_2 protection layers that were in turn used as a mask for selective deposition of Ni-Mo compounds at specific areas of the SiNW arrays [35]. Unfortunately, this SiO_2 patterning approach relies heavily on lithography and is not possible through the means of conventional chemical or electrochemical oxidation.

The goal of the present work is to develop a relatively inexpensive and reproducible method of forming localized indium deposits in the bottommost parts of porous silicon layers to be used as seed layers for subsequent ec-LLS growth of germanium crystallites inside the pores. To achieve the fusible metal's localization, we have evaluated the process of its electrochemical deposition into arrays of SiNWs obtained by MACE while taking into account the previously noted specific features of its nucleation on semiconductor substrates that make it stand out from other typically electrodeposited metals, and proposed a suitable approach to provide reproducible indium particle deposition in the bottommost part of the each consecutive pore while also avoiding surface and subsurface deposition.

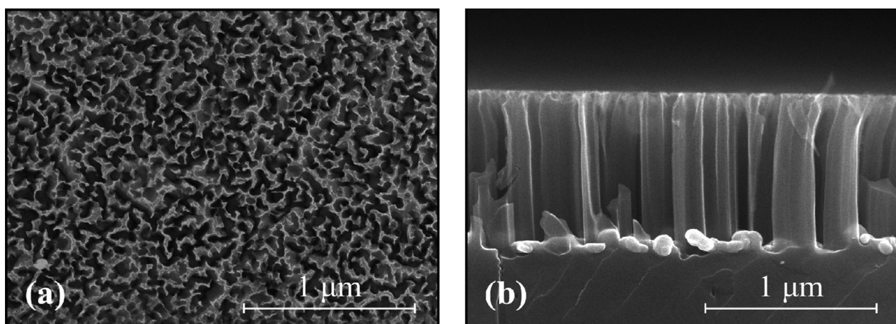

Fig. 2. (a) Surface and (b) cross-section SEM images illustrating the typical structure of initial MACE-produced SiNW arrays with residual silver particles utilized as substrates for indium deposition.

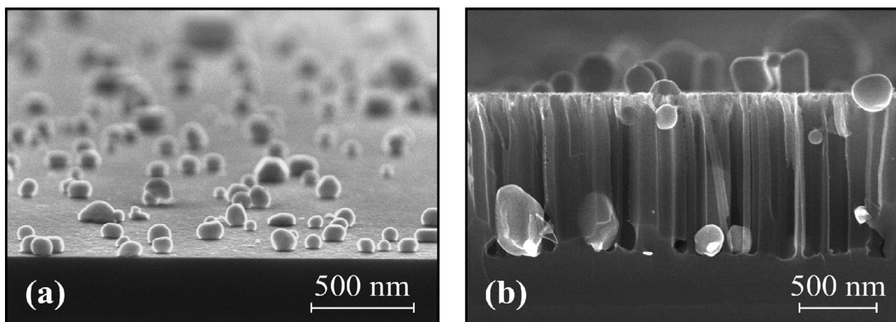

Fig. 3. Cross-section image showcasing the well-separated spatial distribution of indium droplets deposited at 0.5 mA/cm^2 for 10 min onto (a) monocrystalline silicon and (b) SiNW arrays produced by MACE with residual Ag particles preliminarily removed in 20% HNO_3.

2. Materials and methods

All the necessary chemical and electrochemical processing stages were carried out at room temperature (22 °C) using a polytetrafluoroethylene (PTFE) electrochemical cell with a graphite plate in contact with the back of the working electrode and an indium counter-electrode.

Lightly boron-doped (12 Ohm•cm) monocrystalline (100)-oriented silicon wafers were used as working electrodes, which were preliminarily cleaned in chromic acid and subsequently exposed to 4.5% HF to remove the natural oxide layer. A basic two-stage MACE process was carried out to form the initial PS layer. At the first MACE stage, silver particles were chemically deposited onto the silicon wafer's surface for 60 s from a 10 mM $AgNO_3$ aqueous solution with the addition of 3 M HF to embed the deposits into the wafer and 1.17 M ethanol to improve surface solubility. At the second stage, the samples with silver particles were exposed to an aqueous solution containing 4.37 M HF and 0.28 M H_2O_2 (serving as the etchant and oxidant, respectively) for 30 min. To evaluate the role of Ag particles on indium's electrodeposition, we also examined the case where they were not present in the MACE-produced samples by chemically dissolving them in 20% HNO_3 for 5 min subsequently to MACE, followed by an additional stage of SiO_2 removal in 4.5% HF.

Finally, indium was electrodeposited into the obtained porous material from an aqueous solution containing 0.038 M $In_2(SO_4)_3$ and 0.023 M Na_2SO_4 in continuous and pulsed galvanostatic modes at a cathodic current density of 0.5 mA/cm^2 using a Metrohm Autolab PGSTAT302N potentiostat. The working electrode potential measurements during deposition have been conducted in relation to an Ag/AgCl reference electrode. Morphological parameters of the samples were analyzed using a Hitachi S-4800 scanning electron microscope (SEM). The distribution of silver and indium in the resulting deposits was evaluated using a Bruker QUANTAX 200 energy-dispersive X-ray analyzer (EDX), acquiring element spatial distribution maps overlaid over their corresponding SEM images. For distribution comparison, element concentration profiles were obtained by scanning each sample diagonally across the porous layer. It should be noted that this particular method of elemental analysis relies on acquiring the X-ray spectra from a volume of around 0.5 μm^3. Since the structures in question generally fall below this size threshold, the data obtained via this method (EDX concentration profiles and EDX maps) can be perceived as average throughout said volume and are therefore expressed in arbitrary units (a.u.). As the conditions of the EDX analysis remained unchanged for all the samples discussed in the present work, we consider this approach reasonable due to only using these concentration values as means of spatial distribution comparison [26].

3. Results

As a result of carrying out the MACE process, arrays of 1 μm-long vertically-aligned SiNWs were formed. Since the silver particles in the initial mask were rather separated, the nanowires in the arrays are interconnected, forming a silicon skeleton similar to that of anodic PS, with residual Ag particles located at the very bottoms of the resulting pore channels (Fig. 2).

Prior to the results obtained on MACE-fabricated SiNW arrays with Ag particles, we have studied the features of indium's continuous and pulse-mode electrochemical deposition onto monocrystalline silicon and various types of PS, including SiNWs with the residual Ag particles chemically removed in HNO_3. It has been found that, regardless of the chosen deposition regime, indium particles tend to deposit in relatively large well-separated droplet-like clusters (Fig. 3, a), which in the case of SiNWs without any residual metal particles (Fig. 3, b) results in surface and subsurface deposition, in addition to not each subsequent pore channel being filled. After prolonged electrolysis, the separated indium particles grow vertically upwards as opposed to interconnecting and forming a continuous film. The number of initial nuclei can most likely be increased by drastically raising the deposition current density [27], but that comes at a cost of a significantly increased overall thickness of the resulting film and the emergence of surface and subsurface deposition, making this approach inapplicable in the case of filling a porous material.

A comparison of experimental results obtained after continuous galvanostatic electrochemical deposition of indium onto SiNW arrays formed by MACE at two different deposition times is compiled in Fig. 4, a, b, demonstrating a clear beneficial effect of residual silver particles on deposit localization. To minimize the effect of diffusion limitations,

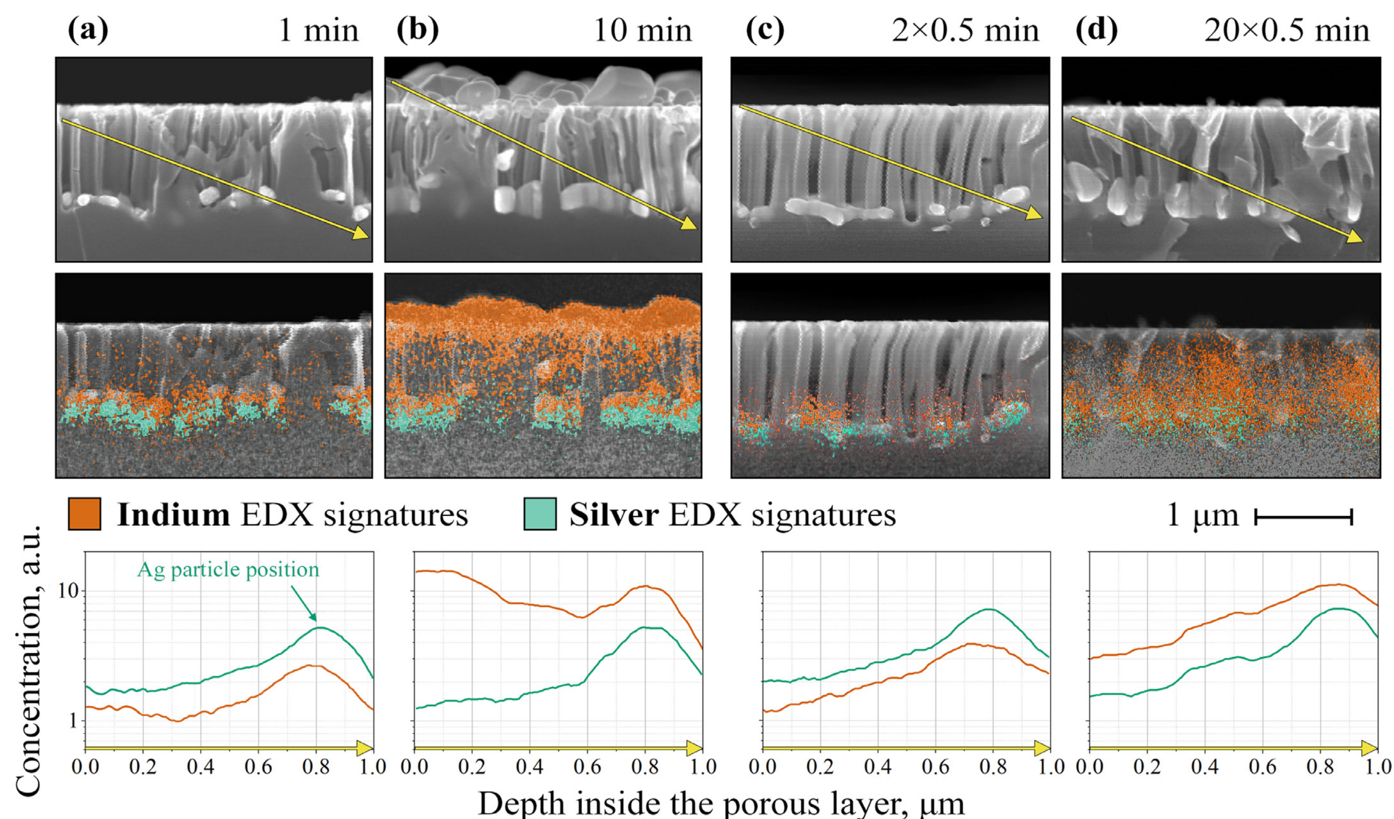

Fig. 4. SEM images (top row), EDX maps overlaid over SEM images (middle row), and indium and silver concentration profiles (bottom row) of MACE-produced SiNW arrays after (a, b) continuous and (c, d) pulsed-mode indium electrodeposition at 0.5 mA/cm^2.

we also attempted to deposit indium using current pulses separated by 120 s pauses to give the solution inside the pores ample periods of time to refresh before each successive pulse, with the according results compiled in Fig. 4, c, d. SEM images of the samples, with the exception of surface and subsurface deposition in the case of prolonged continuous deposition, demonstrate well-defined spherical metal particles located at the bottoms of the pore channels. A clear separation between indium and silver deposits inside the pores is difficult to determine, as the two metals have nearly identical appearances in SEM images, and the spatial resolution of the EDX technique does not allow to point out a clear boundary between the two signatures. As such, the amount of indium can only be deducted by means of comparison to the results presented in Fig. 2.

Since the main advantage of the pulsed-mode deposition is the presence of pauses that counter diffusion limitations, the duty cycle D (the ratio between the pulse duration and the period) is one of the most crucial parameters when it comes to pore filling.

The results obtained by utilizing adjusted pulsed-mode deposition regimes with various D values while maintaining the same overall charge (or the same deposition time, since the current density remained unchanged) are presented in Fig. 5 and demonstrate a notable reduction in surface deposit density along with D.

The difference in working electrode potential with time recorded during indium electrodeposition into PS samples formed by MACE is illustrated by Figs. 6 and 7.

4. Discussion

overall distribution of indium deposits on both monocrystalline and porous silicon are in significant contrast to the more commonly electrodeposited metals [12, 19, 20–22]. The small number of initial indium nuclei notable on most of the SEM images points towards the low wettability of silicon's surface by metallic indium, and indicates the latter's growth in accordance with the Vollmer–Weber mechanism. This is likely to be one of the primary reasons preventing effective and reproducible pore filling in the case of anodic PS [25, 26].

We presume that indium nucleation initiates at points where a local breakdown of the dielectric layer occurs. In the case of silicon, the breakdown can be assumed to occur at points where the natural SiO_2 layer is at its thinnest. The EDX mapping data and SEM images of the samples obtained by galvanostatic electrochemical indium deposition into SiNWs arrays formed by MACE (Figs. 4 and 5) in direct comparison with the results obtained on SiNWs without residual silver particles (Fig. 2) confirm our assumptions in regards to the latter acting as nucleation points whereat indium electrodeposition primarily occurs. Silver particles pose much more energy effective points for indium nucleation, since no oxide breakdown is required for the nuclei to form. In addition to that, the silver particles' surfaces also don't share silicon's issue of low wettability. As such, indium is primarily deposited at the pore bottoms, with an exception of surface and subsurface deposition present at increased durations.

Indium deposits obtained after a brief 1 min electrodeposition process (in the cases of both continuous and pulsed deposition) are localized predominantly at the surfaces of the residual silver particles (Fig. 4, a, c). The combined deposits' diameters remain close to those of the initial silver particles and range from 70 to 150 nm. EDX-based concentration profiles exhibit an almost identical spatial distribution of the two metals, with silver's signature (1.4 a.u. in the subsurface area and 4.3 a.u. at the pore bottoms) being noticeably more pronounced than indium's (0.9 and 2.2 a.u., respectively). Based on these results, it can be assumed that the sizes of indium clusters obtained at such a small deposition time are insignificant compared to the much larger silver particles underneath them, making them unsuitable for ec-LLS.

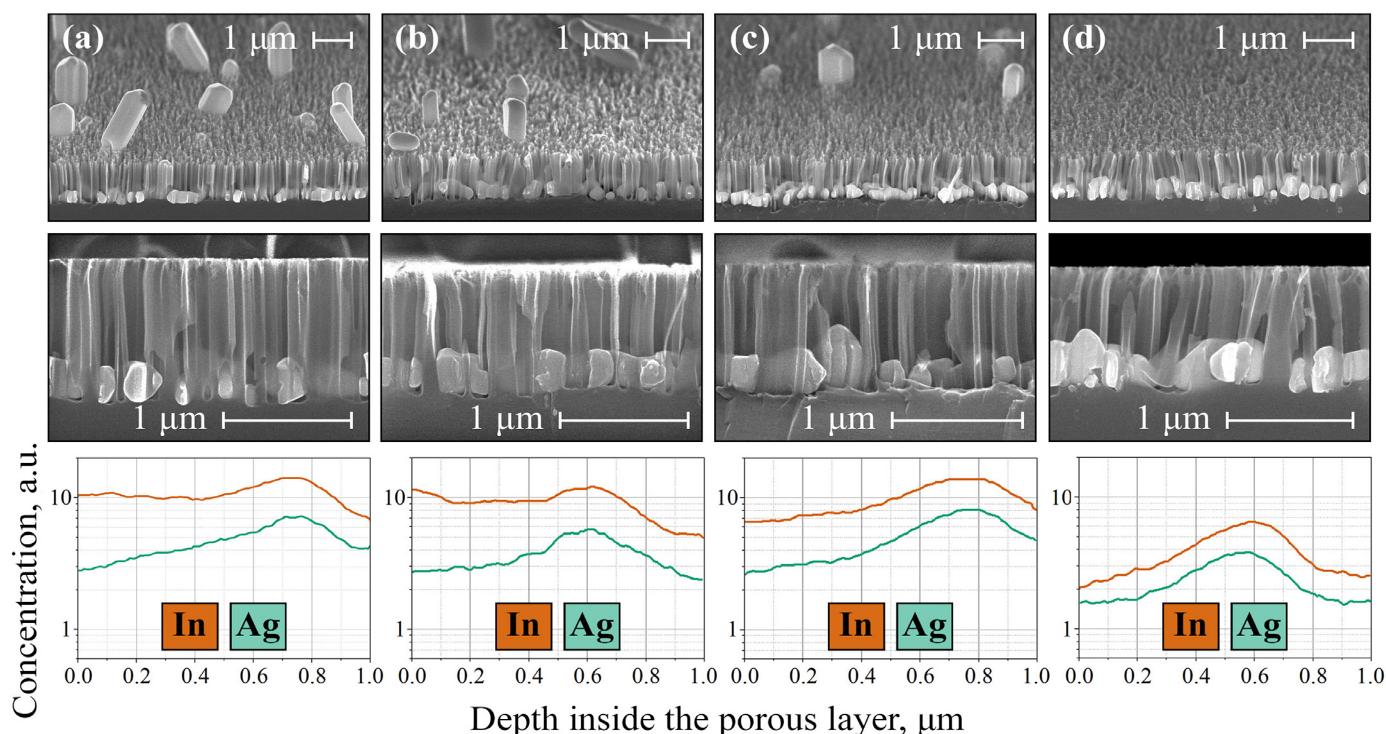

Fig. 5. SEM images (top two rows) and indium and silver concentration profiles (bottom row) of MACE-produced SiNW arrays after depositing indium at 0.5 mA/cm^2 in various pulse-mode regimes: (a) twenty 30 s pulses with 120 s pauses ($D = 0.200$), (b) forty 15 s pulses with 120 s pauses ($D = 0.111$), (c) two hundred 3 s pulses with 24 s pauses ($D = 0.111$) (d) two hundred 3 s pulses with 120 s pauses ($D = 0.024$).

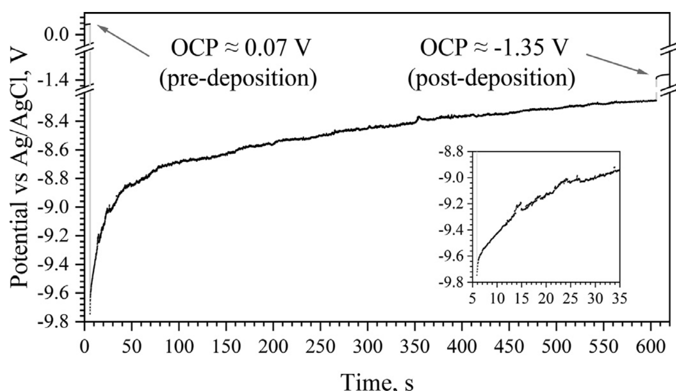

Fig. 6. Working electrode potential dependence on processing time in the case a 10-minute stationary galvanostatic (−0.5 mA/cm^2) deposition process. The deposition was initiated at a 5 s mark and ended at 605 s. The zoomed inset shows the initial 30 s of the deposition process.

Attempting to raise the pore filling factor by simply increasing the deposition time tenfold while using the same MACE-produced substrate causes the indium deposits to accumulate into larger (up to 350 nm) vertical structures within the pores (11 a.u.), but also creates a comparatively rich (14 a.u.) layer of indium particles at the surface and in the subsurface areas of the porous layer (Fig. 4, b). The sizes of particles present on the surface are noticeably larger (up to 800 nm) than the diameters of the pores themselves, with each particle covering up multiple pores from above, indicating that indium also nucleates in subsurface areas where their growth initiates. This change in the deposit distribution can presumably be attributed to the diffusion limitations brought forward by the small lateral sizes of pores in-between the adjacent nanowires, which greatly complicates the diffusion of reagents and reaction byproducts into and out of the pores and effectively halts the deposition solution renewal.

SEM images presented in Fig. 4, d revealed that the use of twenty 30-second pulses of 0.5 mA/cm^2 separated by 120-second zero current pauses (which amounts to the same total deposition time of 10 min) made it possible to minimize the surface and subsurface deposition (down to 3 a.u. in terms of EDX signatures) otherwise present after a 10-minute deposition process, almost exclusively localizing the deposits on the silver particles within the pores (up to 12 a.u.). While the amount of indium inside the pores can be deemed optimal, nucleation still occurs at select portions of the sample's surface, more clearly visible on its other cross-sections (Fig. 5, a), resulting in scarce yet large surface indium deposits and thus requiring certain alterations to the processing parameters to be made.

As the results presented in Fig. 5 would indicate, by maintaining the same overall charge and varying the pulse and pause duration (or the duty cycle value D), various cases of indium distribution can be achieved. Fig. 5, a, b, c all showcase the presence of large indium crystallites on the surface of the porous layer, with their spatial concentration gradually decreasing along with D. While it's hard to determine whether or not their growth initiated at the pore bottoms or at the surface, their sheer size makes these structures inapplicable for subsequent ec-LLS, as the surface germanium deposits would greatly outnumber those inside the pores, making reproducible acquisition of SiGe alloys impossible. By minimizing D to the value of around 0.1 (Fig. 5, d), surface and subsurface deposition is completely eliminated, providing complete deposit localization at the pore bottoms.

As the time-potential graphs presented in Figs. 6 and 7 would suggest, indium nucleation occurs in the first half of the allotted deposition time, followed by subsequent growth of the already formed nuclei. This is especially apparent from the open-circuit potential (OCP) values recorded during the pause after the 8th consecutive pulse (Fig. 7, d): indium's presence affects the surface potential of the working electrode, but due to the solution's acidic nature the scarce indium nuclei are

Fig. 7. Working electrode potential dependence on processing time in the case of employing 20 consecutive cathodic current (−0.5 mA/cm^2) pulses of 30 s each separated by 120 s pauses. The first pulse was initiated at a 100 s mark. The colored insets correspond to the few select pulse-pause sequences (a-b, c-d, e-f) correspondingly highlighted on the primary graph.

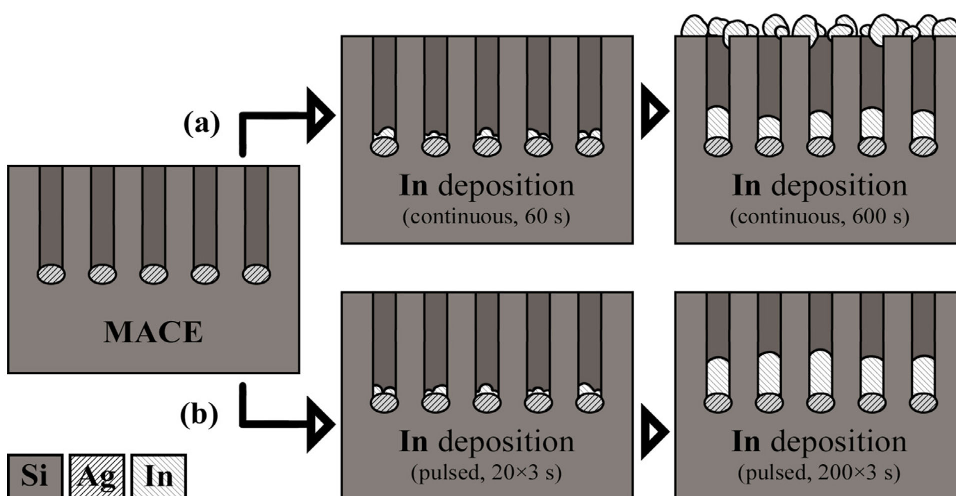

Fig. 8. Schematic illustration of the sequential indium deposition stages into MACE- produced SiNW arrays for the cases of indium's (a) continuous deposition and (b) pulsed-mode deposition with optimized duty cycle.

easily dissolved, indicated by OCP returning to its original value. The deposit accumulates in size towards the end of the process (Fig. 7, f) and becomes significantly more stable, with long-term OCP values directly corresponding to those obtained during stationary deposition (Fig. 6, c). Post-deposition OCP is not significantly affected by the presence of surface deposits, remaining in the range of −1.30 to −1.40 V regardless of the selected pulsed-mode deposition parameters such as the duty cycle.

Most of the observed indium deposition results can be divided into two basic generalized cases, as illustrated by Fig. 8.

While the initial stages of deposition for both stationary and pulsed-mode regimes seem to result in roughly the same overall indium distribution, the amount of metal present at the pore bottoms is not yet significant enough for its effective application in ec-LLS and would result in non-uniform pore filling with germanium. Indium distribution in the cases of prolonged stationary deposition (Fig. 8, a) can also be deemed suboptimal for subsequent ec-LLS, as germanium's growth will primarily occur in the surface and subsurface areas, soon blocking the route for reagent and byproduct transfer into and out of the pore channels (Fig. 1). Increasing the amount of metal at the pore bottoms without also causing surface nucleation can only be achieved by pulse-mode deposition (Fig. 8, b). It's also important to maintain a low duty cycle value by utilizing shorter pulses and/or longer pauses: as the duty cycle value decreases (starting with the continuous electrodeposition which is equivalent to a pulsed-mode regime with $D = 1$), the solution within the pores is given more and more time to replenish after each successive pulse, gradually decreasing the input of diffusion limitations that occur due to the solution's local depletion.

5. Conclusion

As a part of the present work, we have proposed a previously unexplored approach to localized indium electrodeposition into silicon nanowire arrays that allows elimination of surface and subsurface deposits that are generally present when depositing this metal onto anodic porous silicon layers. Evidently, by employing MACE-fabricated arrays of lightly-doped SiNWs as porous matrices for subsequent pulse-mode electrochemical deposition of indium, complete deposit localization at the bottoms of the pore channels (on the residual silver particles previously used for MACE) can be achieved as long as an optimal ratio of current density and deposition time is maintained. Of all the relevant pulse-mode deposition parameters, the duty cycle value should be taken into account and reduced firsthand, as the presence of indium on the surface is directly dictated by diffusion limitations that arise when the pulse duration is too high or the pause duration is too low. In comparison with stationary electrodeposition, a notable improvement on deposition selectivity is observed in adjusted pulsed-mode deposition regimes, allowing current densities or overall deposition times to be increased, as pauses between current pulses allow the deposition solution within the pores to be replenished, preventing any deposition on the surface or in subsurface regions.

Evidently, by maintaining a low duty cycle value and varying the overall deposition duration, any degree of pore filling inside MACE-produced PS can be achieved, in contrast to the fine scattered indium particles and irregular pore filling usually observed on anodic PS. This seems to offer tempting prospects for the use of such structures as substrates for subsequent germanium deposition via ec-LLS. Presumably, PS layers with indium particles of sufficient size localized exclusively at the pore bottoms can be used to provide favorable conditions for subsequent filling of pore channels with crystalline germanium via the ec-LLS approach, followed by thermal annealing of the resulting structures in order to form Si_xGe_{1-x} alloys, with the component ratios in the latter being directly dependent on structural parameters of the initial porous layers. An evaluation of such a possibility is currently underway.

Funding

This research was supported by the Russian Science Foundation (project №20–19–00720).

Declaration of Competing Interest

The authors declare that they have no known competing financial interests or personal relationships that could have appeared to influence the work reported in this paper.

Acknowledgments

We would like to thank D. Zhigulin (State Center "Belmicroanalysis", Affiliate Research & Design Center "Belmicrosystems", JSC "INTEGRAL", Minsk, Belarus) for performing SEM and EDX analyses of the experimental samples. V. Yakovtseva's help in proof-reading, editing and providing thorough advice on improving the manuscript text is strongly acknowledged.

References

[1] E. Chubenko, S. Redko, A. Dolgiy, H. Bandarenka, S. Prischepa, V. Bondarenko, G Korotcenkov, in: Porous Silicon: From Formation to Application, Taylor & Francis Group, Boca Raton, 2016, p. 181. Editor.
[2] G. Korotcenkov, Porous Silicon: From Formation to Application, Taylor & Francis Group, Boca Raton (2016), P. 12, doi:10.1201/b19342.
[3] J. Yang, T. Caillat, Thermoelectric Materials for Space and Automotive Power Generation, MRS Bull. 31 (2006) 224–229, doi:10.1557/mrs2006.49.
[4] A. Usenko, D. Moskovskikh, Gorshenkov M, A. Voronin, A. Stepashkin, S. Kaloshkin, D. Arkhipov, V. Khovaylo, Enhanced thermoelectric figure of merit of p-type $Si_{0.8}Ge_{0.2}$ nanostructured spark plasma sintered alloys with embedded SiO_2 nanoinclusions, Scr. Mater. 127 (2017) 63–67, doi:10.1016/j.scriptamat.2016.09.010.
[5] E. Fahrenkrug, J. Biehl, S. Maldonado, Electrochemical Liquid–Liquid–Solid Crystal Growth of Germanium Microwires on Hard and Soft Conductive Substrates at Low Temperature in Aqueous Solution, Chem. Mater. 27 (9) (2015) 3389–3396, doi:10.1021/acs.chemmater.5b00644.
[6] I.M. Gavrilin, D.G. Gromov, A.A. Dronov, S.V. Dubkov, R.L. Volkov, A. Yu. Trifonov, N.I. Borgardt, S.A. Gavrilov, Effect of electrolyte temperature on the cathodic deposition of Ge nanowires on in and Sn particles in aqueous solutions, Semiconductors 51 (2017) 1067–1071, doi:10.1134/S1063782617080115.
[7] S. Acharya, L. Ma, S. Maldonado, Critical Factors in the Growth of Hyperdoped Germanium Microwires by Electrochemical Liquid–Liquid–Solid Method, Applied Nano Materials 1 (10) (2018) 5553–5561, doi:10.1021/acsanm.8b01068.
[8] Q. Cheek, E. Fahrenkrug, S. Hlynchuk, D.H. Alsem, N.J. Salmon, S. Maldonado, In Situ Transmission Electron Microscopy Measurements of Ge Nanowire Synthesis with Liquid Metal Nanodroplets in Water, ACS Nano 14 (3) (2020) 2869–2879, doi:10.1021/acsnano.9b06468.
[9] L. Ma, S. Lee, J. DeMuth, S. Maldonado, Direct electrochemical deposition of crystalline silicon nanowires at T≥60°C, RSC Adv. 6 (2016) 78818–78825, doi:10.1039/C6RA13378A.
[10] N. Downes, Q. Cheek, S. Maldonado, Electroreduction of Perchlorinated Silanes for Si Electrodeposition, J. Electrochem. Soc. 168 (2) (2021), doi:10.1149/1945-7111/abda58.
[11] E. Fahrenkrug, J. Gu, S. Maldonado, Electrodeposition of Crystalline GaAs on Liquid Gallium Electrodes in Aqueous Electrolytes, J. Am. Chem. Soc. 135 (1) (2013) 330–339, doi:10.1021/ja309476x.
[12] A. Dolgiy, S.V. Redko, H. Bandarenka, S.L. Prischepa, K. Yanushkevich, P. Nenzi, M. Balucani, V. Bondarenko, Electrochemical Deposition and Characterization of Ni in Mesoporous Silicon, J. Electrochem. Soc. 159 (10) (2012), doi:10.1149/2.050210jes.
[13] F. Hamadache, C. Renaux, J.-.L. Duvail, P. Bertrand, Interface investigations of iron and cobalt metallized porous silicon: AES and FTIR analyses, Physica Status Solidi A 197 (1) (2003) 168–174, doi:10.1002/pssa.200306494.
[14] C. Renaux, V. Scheuren, D. Flandre, New experiments on the electrodeposition of iron in porous silicon, Microelectron. Reliab. 40 (4–5) (2000) 877–879, doi:10.1016/S0026-2714(99)00331-5.
[15] R. Hérino, P. Jan, G. Bomchil, Nickel Plating on Porous Silicon, J. Electrochem. Soc. 132 (1985), doi:10.1149/1.2113612.
[16] P. Granitzer, K. Rumpf, S. Surnev, H. Krenn, Squid-magnetometry on ferromagnetic Ni-nanowires embedded in oriented porous silicon channels, J. Magn. Magn. Mater. 290 (1) (2005) 735–737, doi:10.1016/j.jmmm.2004.11.359.
[17] E. Michelakaki, K. Valalaki, A.G. Nassiopoulou, Mesoscopic Ni particles and nanowires by pulsed electrodeposition into porous Si, J. Nanopart. Res. 15 (2013) 1499, doi:10.1007/s11051-013-1499-3.
[18] E.B. Chubenko, S.V. Redko, A.I. Sherstnyov, V.A. Petrovich, D.A. Kotov, V.P. Bondarenko, Influence of the Surface Layer on the Electrochemical Deposition of Metals and Semiconductors into Mesoporous Silicon, Semiconductors 50 (2016) 372–376, doi:10.1134/S1063782616030040.

[19] K. Rumpf, P. Granitzer, M. Albu, P. Poelt, Electrochemically Fabricated Silicon/Metal Hybrid Nanosystem with Tailored Magnetic Properties, Electrochem. Solid State Lett. 13 (2010) 2, doi:10.1149/1.3269188.
[20] K. Fukami, K. Kobayashi, T. Matsumoto, Y.L. Kawamura, T. Sakka, Y.H. Ogata, Electrodeposition of Noble Metals into Ordered Macropores in p-Type Silicon, J. Electrochem. Soc. 155 (6) (2008), doi:10.1149/1.2898714.
[21] P. Granitzer, K. Rumpf, Filling of porous silicon with magnetic materials, Semicond. Sci. Technol. 31 (1) (2016), doi:10.1088/0268-1242/31/1/014004.
[22] R. Koda, K. Fukami, T. Sakka, Y. Ogata, Electrodeposition of platinum and silver into chemically modified microporous silicon electrodes, Nanoscale Res. Lett. 7 (2012), doi:10.1186/1556-276X-7-330.
[23] K. Fukami, R. Koda, T. Sakka, Y. Ogata, M. Kinoshita, Electrochemical deposition of platinum within nanopores on silicon: Drastic acceleration originating from surface-induced phase transition, J. Chem. Phys. 138 (9) (2013), doi:10.1063/1.4793526.
[24] P. Granitzer, K. Rumpf, Porous Silicon—A Versatile Host Material, Materials 3 (2) (2010) 943–998, doi:10.3390/ma3020943.
[25] N.L. Grevtsov, E.B. Chubenko, V.P. Bondarenko, I.M. Gavrilin, A.A. Dronov, S.A. Gavrilov, The Effect of Porous Silicon Oxidation on Electrochemical Formation of Porous Silicon–Indium Nanocomposites, Tech. Phys. Lett. 47 (4) (2021), doi:10.1134/S1063785021040088.
[26] N. Grevtsov, E. Chubenko, V. Bondarenko, I. Gavrilin, A. Dronov, S. Gavrilov, Electrochemical deposition of indium into oxidized and unoxidized porous silicon, Thin. Solid. Films 734 (2021), doi:10.1016/j.tsf.2021.138860.
[27] P. Lobacarro, A. Raygani, A. Oriani, N. Miani, A. Piotto, R. Kapadia, M. Zheng, Z. Yu, L. Magagnin, D. Chrzan, R. Maboudian, A. Javey, Electrodeposition of High-Purity Indium Thin Films and Its Application to Indium Phosphide Solar Cells, J. Electrochem. Soc. 161 (2014), doi:10.1149/2.0821414jes.
[28] N. Grevtsov, A. Burko, S. Redko, N. Khinevich, S. Zavatski, S. Niauzorau, H. Bandarenka, MRS Advances 5 (2020) 2023–2032, doi:10.1557/adv.2020.332.
[29] Z. Huang, N. Geyer, P. Werner, J. de Boor, U. Gösele, Metal-Assisted Chemical Etching of Silicon: A Review, Adv. Mater. 23 (2011) 285–308, doi:10.1002/adma.201001784.
[30] H. Han, Z. Huang, W. Lee, Metal-assisted chemical etching of silicon and nanotechnology applications, Nano Today 9 (3) (2014) 271–304, doi:10.1016/j.nantod.2014.04.013.
[31] R. Lai, T. Hymel, V. Narasimhan, Y. Cui, Schottky Barrier Catalysis Mechanism in Metal-Assisted Chemical Etching of Silicon, Applied Materials and Interfaces 8 (14) (2016) 8875–8879, doi:10.1021/acsami.6b01020.
[32] C. Lee, S. Tsuru, Y. Kanda, S. Ikeda, M. Matsumura, Formation of 100 μm Deep Vertical Pores in Si Wafers by Wet Etching and Cu Electrodeposition, J. Electrochem. Soc. 156 (12) (2009), doi:10.1149/1.3237139.
[33] S. Yae, K. Sakabe, N. Fukumuro, S. Sakamoto, H. Matsuda, Surface-Activation Process for Electroless Deposition of Adhesive Metal (Ni-B, Cu) Films on Si Substrates Using Catalytic Nanoanchors, J. Electrochem. Soc. 158 (9) (2011), doi:10.1149/1.3610221.
[34] T. Ozel, B. Zhang, R. Gao, R. Day, C. Lieber, D. Nocera, Electrochemical Deposition of Conformal and Functional Layers on High Aspect Ratio Silicon Micro/Nanowires, Nano Lett. 17 (7) (2017) 4502–4507, doi:10.1021/acs.nanolett.7b01950.
[35] F. Wendisch, M. Abazari, V. Werner, H. Barb, M. Rey, E. Goerlitzer, N. Vogel, H. Mahdavi, G. Bourret, Spatioselective Deposition of Passivating and Electrocatalytic Layers on Silicon Nanowire Arrays, Applied Materials and Interfaces 12 (47) (2020), doi:10.1021/acsami.0c14013.